ELSEVIER

Journal of Archaeological Science 34 (2007) 771–780

Journal of Archaeological SCIENCE

http://www.elsevier.com/locate/jas

Edge damage distribution at the assemblage level on Middle Stone Age lithics: an image-based GIS approach

Catherine Bird [a], Tom Minichillo [b,*], Curtis W. Marean [c]

[a] *School of Human Evolution and Social Change, PO Box 872402, Arizona State University, Tempe, AZ 85287-2402, USA*
[b] *Department of Anthropology, University of Washington, Seattle, USA*
[c] *Institute of Human Origins, School of Human Evolution and Social Change, PO Box 872402, Arizona State University, Tempe, AZ 85287-2402, USA*

Received 3 April 2006; received in revised form 17 August 2006; accepted 22 August 2006

Abstract

Lithic artifacts represent the most abundant cultural remains from Middle Stone Age sites in southern Africa. Of these, pointed forms (under a variety of names), blades, and flakes have long been recognized as the three most abundant general types, and retouch on all three is rare relative to similar forms of equivalent age elsewhere. Here we offer a new technique for documenting concentrations of edge damage on an assemblage level to infer taphonomic processes and to record usewear and retouch. This approach is specifically aimed at patterning on the assemblage scale, rather than on individual artifacts. We use points from a Middle Stone Age assemblage from Pinnacle Point Cave 13B, near Mossel Bay, South Africa, to illustrate the technique. Combining GIS, rose diagrams, and polar statistics, we were able to visually and statistically summarize lithic artifacts for patterns of edge damage. For the points made on quartzite in this assemblage, edge damage was found to be significantly patterned and taphonomic causes of the damage were rejected. The technique also opens avenues for many other quantitative analyses that are either impossible or difficult with current non-visual systems of recording, such as measurements of distance, angle, and area of edge damage.

Keywords: Middle Stone Age; Lithics; Edge damage; GIS; Image Analysis; Taphonomy

1. Introduction

The Middle Stone Age (MSA) is a broad technologically and temporally defined period of African archaeology, beginning at least 300,000 years ago (Tryon and McBrearty, 2006) and persisting in some parts of Africa as late as 25,000 years ago (Villa et al., 2005; Wadley and Vogel, 1991). It is marked by increasing technological and symbolic sophistication (Henshilwood et al., 2001, 2002, 2004; Yellen, 1996) and the first appearance of *Homo sapiens* (McDougall et al., 2005; White et al., 2003). The MSA is currently a topic of discussion that is mostly focused its importance in understanding the origin of our species (Henshilwood and Marean, 2003; Klein, 1992; McBrearty and Brooks, 2000). This paper does not address that topic and instead utilizes the data from an MSA assemblage to illustrate a methodological approach. Overviews and current discussions of the MSA are available elsewhere (Barham, 2000; Deacon and Deacon, 1999; Henshilwood and Marean, 2003; Klein, 1999; McBrearty and Brooks, 2000; Mitchell, 2002; Wurz, 2002; Wurz et al., 2003, 2005). MSA people in southern Africa produced toolkits containing points, bifacial points, unifacial points, scrapers, blades, bladelets, flakes, and backed blades (Shea, 2006; Singer and Wymer, 1982; Thackeray, 1992; Wurz, 2002). MSA toolkits are dominated by unretouched pieces, with retouch often restricted in distribution and intensity (Volman, 1981). This is in contrast to many Eurasian Middle Paleolithic sites of similar age, where retouched pieces are

* Corresponding author. 2323 NE 86th Street, Seattle, WA 98115, USA. Tel./fax: +1 206 525 7404.
E-mail addresses: kiwiyama@aol.com (C. Bird), tom.minichillo@hotmail.com (T. Minichillo), curtis.marean@asu.edu (C.W. Marean).

0305-4403/$ - see front matter © 2006 Elsevier Ltd. All rights reserved.
doi:10.1016/j.jas.2006.08.005

common and retouch can be intensive (Debénath and Dibble, 1994). In South African MSA assemblages, lithic pieces often have very slight edge damage that grades into a pattern resembling retouch or focused use with resulting edge damage (Keeley, 1980; Vaughan, 1985). The lithics from Site 13B at Pinnacle Point show this pattern.

There are two likely causes of this lighter edge damage: (1) natural processes such as trampling, water tumbling, or sedimentary compaction, or (2) human use. It has been argued that random edge damage is suggestive of non-behavioral causes, such as trampling or water tumbling (Tringham et al., 1974). If patterned, however, human behavior is implied. While these arguments have yet to be fully demonstrated in every case, we accept them here as a starting point. Additional experimental work that records edge damage in the manner proposed in this paper may further the specifics of that debate. A difficulty in assessing these patterns for randomness comes from their complex geometries and the difficulty in precisely recording edge damage locations. Earlier evaluations of randomness in edge damage distributions have been largely subjective (Bordes, 1961; Flenniken and Haggerty, 1979; McBrearty et al., 1998; Newcomer, 1976; Tringham et al., 1974). The technique reported here allows for the precise recording of edge damage and the application of statistical tests of whether the null hypothesis, that damage is randomly distributed and thus more likely taphonomic and without behavioral meaning, is supported.

2. Pinnacle Point Cave 13B

At the tip of Pinnacle Point near Mossel Bay are a series of six caves and rockshelters within a stretch of 100 m of cliff space grouped as the site 13 complex (Fig. 1). All are sea caves cut into faults by high sea levels. The cliffs are exposures of the Table Mountain group of quartzitic sandstones, which is the parent material for the majority of the lithics. Rather than made from the bedrock exposure the majority of the quartzite raw materials is made from beach cobbles (Minichillo, 2005). The sea is currently just below the sites, but was likely a variable distance away during their MSA occupation.

Site 13B is a cave with rich MSA deposits that has been the focus of excavation since 2000 (Marean et al., 2004). Excavations have been directed at three areas within the cave; the western (back), eastern (front) and north-eastern (LC-MSA). All three have stratified deposits of MSA occupation, but the precise relation between the three areas has not yet been resolved. We plot all observed artifactual and ecofactual

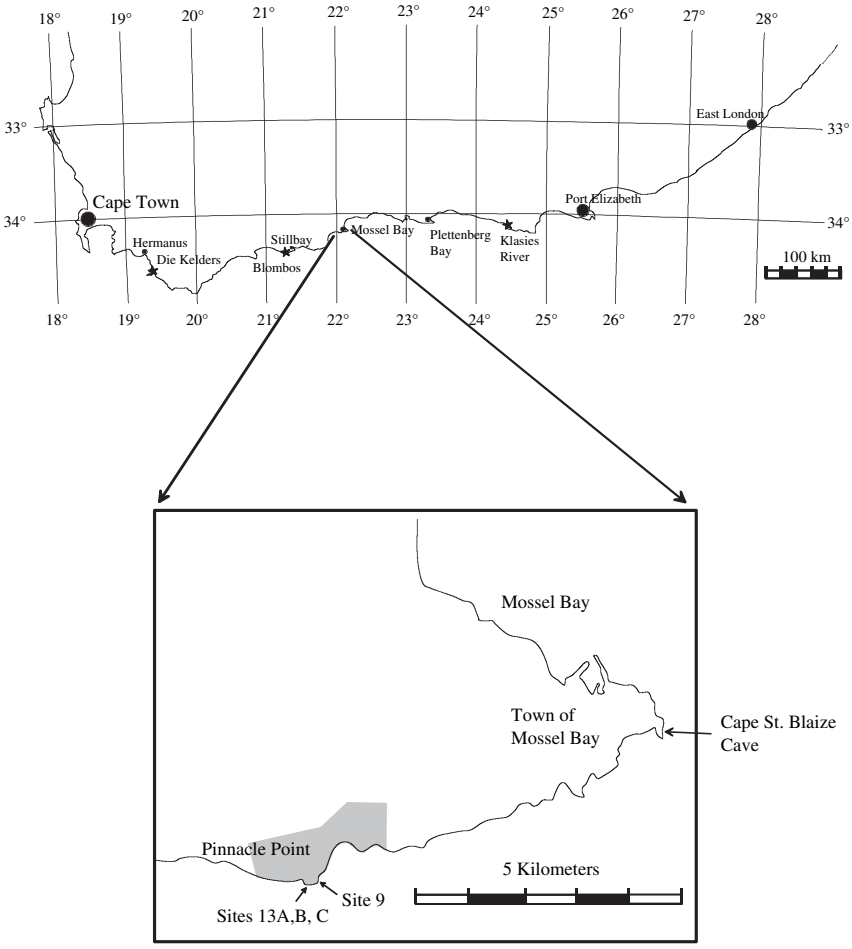

Fig. 1. Map of the Cape coast of southern Africa showing the location of Pinnacle Point Cave 13B.

material directly to total station, though there is a large sample of very small flakes that escapes this plot which is subsequently captured in a set of nested wet screens (10-3-1.5 mm). The analysis to date has focused on this plotted sample, and it is unlikely that whole pieces escaped plotting and made it into the screens.

3. Lithic artifacts at Cave 13B

At Pinnacle Point 13B, the majority (95%) of the plotted lithic artifacts including flakes, convergent flakes, and blades are unretouched pieces, though this percentage could fall if unplotted lithics were included (Marean et al., 2004; Minichillo, 2005). The assemblage is dominated by coarse-grained quartzite, but includes small percentages of other raw materials, such as quartz and silcrete. It is composed of fragmented pieces, whole pieces, (points, blades, and flakes), and cores (Marean et al., 2004; Minichillo, 2005). Here we use only the convergent flakes (sometimes classified as MSA points, Levallois points, or convergent flake-blades) made on quartzite to illustrate the method we are reporting. This was done so that the most abundant raw material class was used, so that differences in edge damage observability based on raw material class would not be a factor and so that some differences in the statistical analysis that could be attributed to general shape are somewhat accounted for. Further accounting for the divergence of the shape of the artifacts analyzed using this method from the assumed circle of the statistical methods applied here could be obtained through experimental studies. This would especially be of importance if comparisons were being attempted between artifacts of generally different shapes.

4. Trampling replication studies

One difficulty in analyzing lithics is separating behavioral components of edge damage associated with use from others, such as trampling and geological processes. Cave sites are often grouped together because of a general preconception that their formation processes and their depositional environments are similar (Barton and Clark, 1993). However, even within caves, location (deep interiors vs. mouths) can dictate varying degrees of deposition and erosion. Post-depositional processes can substantially affect archaeological assemblages, especially in caves where continuing instability and collapse can become agents of damage (McBrearty et al., 1998). Cave 13B has been intermittently occupied from approximately 180,000 years ago to the present, and its sedimentological history has included a wide range of depositional, erosional, and subsidence events. Trampling and geological agents for edge damage thus need to be carefully investigated.

A number of researchers have explored trampling replication, using a variety of raw materials and substrates, to establish diagnostic features of edge damage resulting from taphonomic processes (Bordes, 1961; Flenniken and Haggerty, 1979; Gifford-Gonzalez et al., 1985; Keeley, 1980; Newcomer, 1976; Nielsen, 1991; Pryor, 1988; Shea and Klenck, 1993; Tringham et al., 1974). Each attempted to illustrate how and to what extent the non-behavioral damage might have been inappropriately evaluated as behavioral. In most cases, these studies either attempted to demonstrate how individual artifacts could have been altered to appear retouched through taphonomic process or to identify individual artifacts that could be excluded from behavioral analyses. The method presented here treats each individual edge damage scar (regardless of what artifact it is on) and the total assemblage as the units of analysis.

Taken together these studies provide insight into how trampling affects artifact integrity; nonetheless, there are inconsistencies between their findings. Earlier studies speculated that trampling could be distinguished from usewear because the taphonomic damage occurs, often as elongated scars, along the perimeter of the flake, with no obvious pattern in location, size, or orientation (Flenniken and Haggerty, 1979; Pryor, 1988; Tringham et al., 1974). Alternatively, Gifford-Gonzalez et al. (1985) found that scar orientation was not random and that the number of elongated scars varied, while Shea and Klenck (1993) noted broad, not elongated flake scars. Keeley (1980)) and McBrearty et al. (1998) both found a random and a clustered distribution of damage along the edges, depending on frequency of damage. While Tringham et al. (1974) contended that damage occurred on one side of the flake, McBrearty et al. (1998), Nielsen (1991), Pryor (1988), and Flenniken and Haggerty (1979) all noted that edge damage occurs bifacially. McBrearty et al. (1998), who had the greatest sample size and the greatest number of controls, argued that contrary to Tringham et al. (1974) original findings, taphonomic damage on individual tools can in fact be mistaken for both usewear and retouch. Importantly, these studies suggest that it is virtually impossible to determine whether sparse damage is due to trampling or use of individual artifacts. An alternative to analyzing edge damage on individual lithics is to search for patterns bifacially and on an assemblage level (Lombard et al., 2004; Lombard, 2005a,b), as illustrated in this article.

5. Method

Our method was developed for a field laboratory setting using equipment and software now common at archaeological excavations. Lithic artifacts from the 2003 and 2004 excavations of Cave 13B that were already coded with either retouch or edge damage or both were selected to be included in this project. A total of 31 quartzite convergent flake-blades were drawn randomly from complete specimens so as to provide an initial test of the development and application of this new method, sampled from all three excavation areas so as to get preliminary information from across the site. Our intention is to next code a larger sample so that temporal and spatial variation can be evaluated.

Edge damage originally coded as retouch, that which displayed appropriate size, regularity, and contiguous removals, was subsequently renamed Type 1 edge damage (T^1). Edge damage coded as taphonomic or usewear damage, that displayed removals of irregular shape and size, or noncontiguous

Table 1
Edge damage coding categories

- TYPE 1: size, regularity, and contiguous removal, suggesting retouch
- TYPE 2: irregular shape and size suggesting use-wear or taphonomic processes

removals, usually with smaller scars, was renamed Type 2 edge damage (T^2) for this study (Table 1). The use of the term edge damage for both scars that are thought to be the result of retouch and those that may be from the use of the tool or post-depositional taphonomic processes is not intended to confuse. Rather it is intended to highlight the unknown nature of both the agent and intention behind individual edge damage scars.

Usewear or edge damage studies can take macroscopic or microscopic approaches (Keeley, 1980; Vaughan, 1985) and both approaches have been recently applied to MSA tools (Lombard et al., 2004; Lombard, 2005a; Minichillo, 2005; Rots, 2005; Rots and Van Peer, 2006). For this study a macroscopic approach was utilized. All tools were observed with the naked eye under bright focused light. Individual scars were sometimes checked under a low-powered (3×) hand lens. This method seemed appropriate for the coarse-grained raw materials and scars less than 1 mm across were regularly recorded. However, for finer-grained raw materials a more microscopic approach may be warranted and could be recorded and analyzed using the methodology described here.

The artifacts were coded and entered into all databases based on three categories: shape, raw material, and size. The shape category consisted of flakes, convergent flakes, and blades, while the raw material category included quartzite, quartz, crystal quartz, and silcrete. For this study, we focused only on 31 artifacts of one shape (convergent flakes) and one raw material (quartzite).

With the platform down, the lithic was then assigned to one of the three pre-made metric grids with the origin *x*,*y* coordinates set at 0,0. These grids acted as the photograph backgrounds for rectification of the image to true metric space (Fig. 2a). The centroid of each artifact was determined by calculating the center of mass; a sticky dot was placed over the centroid to align it with the intersection of the center vertical and horizontal lines on the grid. Each artifact was then digitally photographed using a 4 Megapixel Nikon Coolpix 4500. The split body digital camera was mounted on a tripod approximately 41 cm above the bracket sheets, a height that best minimized distortion given the characteristics of the lens and its focal length. Photographs of both the ventral and dorsal faces were taken, with each artifact producing two separate images, so that data could be collected on each face separately.

The images were next brought into ArcView™ GIS 3.3 as image themes. There they were rectified using ESRI Image Analysis based on the metric coordinates of all four corners of the grid. This rectification adjusts the photo to true geometric size. While we did not use the images for metrical analysis, such rectification allows for calculation of precise measurements on distance, angle, and area that would be difficult or impossible to measure with calipers. Next, a vector theme (a precise line drawing) for each face was created as a polygon (Fig. 2b), and individual polygons were produced for each edge damage scar. The platform was also marked using a straight line. Each polygon was described in the table of attributes and the polygons were grouped numerically and by color. This allowed one category to be visually distinguished

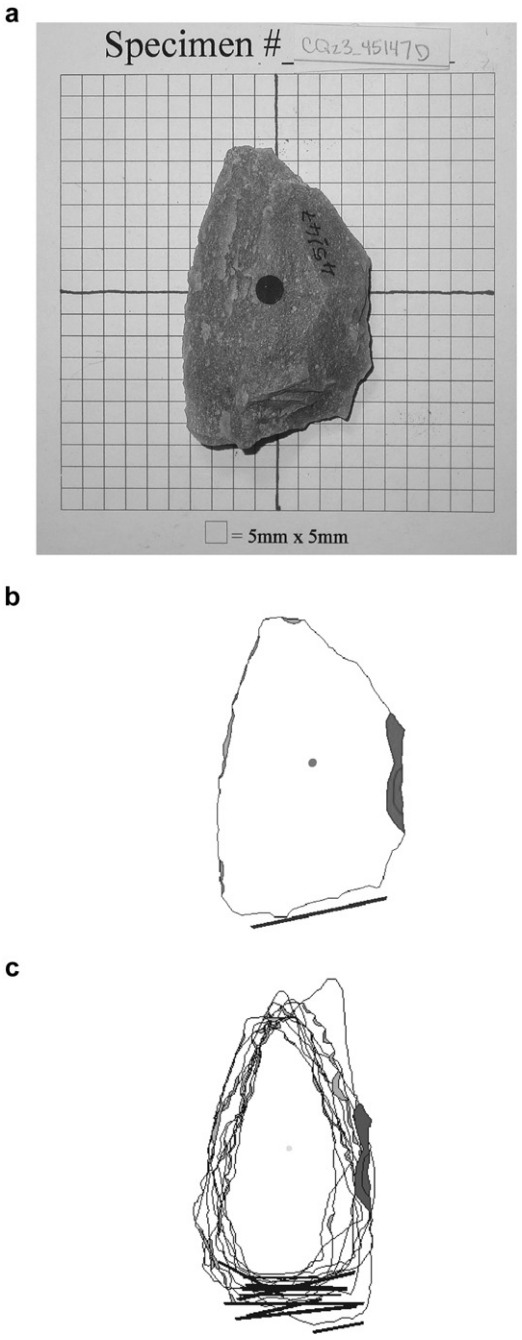

Fig. 2. The process of image rectification, production of vector outlines, and overlap of vector outlines. (a) rectified image of the dorsal face of a quartzite point with the centroid marked, (b) the same quartzite point as a vector (polygon) of the lithic outline and classified damage locations, and (c) composite image of vector maps of the dorsal faces of a series of similarly sized points. The color coding is outline = black, Type 1 edge damage = red, Type 2 edge damage = green, burin damage = blue, and the platform = maroon.

from another (Fig. 2c). Composite maps of either vector (Fig. 2c) or raster type can also be employed to create composite images for shape analysis. These advantages will be explored in future studies, and were part of the original stimulus for the development of the data capture procedures.

6. Rose diagrams

One way to quantify the pattern of edge damage at the assemblage level is to employ rose diagrams. To convert the vector map data to numerical data, Image Tool™, which measures objects on a 360° plane, was employed. With the centroid marked as the intersection between 0° to 180° and 90° to 270°, the length of the edge damage scars were measured individually from the centroid; calculating the arc-angles for each scar individually. The data were recorded at one-degree precision and entered into a master database as ''number of angles.'' The data summary were at the same level of precision as it was entered into the data table (one-degree increments).

Rockworks™, a geology analysis program, was then utilized to create the rose diagrams. Rockworks™ is limited to a precision of five-degree increments when plotting rose diagram petals. This means that a single five-degree flake scar of five one-degree flake scars (in the same five-degree arc) is compiled in the same manner. Nonetheless, the produced rose diagrams are still useful displays that help to visualize patterns in the data, especially when these patterns are validated using statistical tests. Rockworks™ takes the data table of scars and arc-angles and groups them into these five-degree increments, counts the number of scars in each increment, and tallies those for all included specimens. This forms the basis of each rose diagram. ''Bearings'' and ''length'' were used when constructing the rose diagrams and a frequency scale of edge damage was displayed instead of percentages. This was chosen because the percentage scale did not provide information on the sample sizes of the data displayed.

7. Circular statistics

Two circular statistics tests were run on the shape data through the program Oriana™, Kuiper's Test and Rayleigh's Uniformity Test. Kuiper's test compares the distribution of the data to the desired distribution of uniform or von Mises and begins with a null hypothesis that the data follow a random distribution (Fisher, 1993). The test is based on deviation from these desired distributions and gives a ''*V*'' value and a measure of its statistical probability.

After Kuiper's test of randomness has been performed and the null hypothesis has been rejected, Rayleigh's tests for preferred direction can be run. The test begins with a null hypothesis that the data are distributed in a random manner and then calculates the probability that the hypothesis is supported (Fisher, 1993). The test produces a ''*Z*'' value as well as a measure of its statistical significance; a statistically significant result indicates that the data are not distributed uniformly and that they show an unspecified preferred direction (Fisher, 1993). If there is a preferred direction then the null hypothesis is rejected. When the null hypothesis is rejected for both Kuiper's Test and Rayleigh's Test, then the pattern of edge damage is non-random within polar coordinate space. However, the interpretation of the meaning must proceed cautiously and in concert with evaluations of the visual patterning on the rose diagrams, and the structure of the lithic form (for example, points may be less likely to have damage on the platform). These statistics' test for significance of individual diagrams, not strength between diagrams, so the sizes of the *V*-values are not indicative of which rose diagram displays a stronger non-random pattern.

8. Results on convergent flakes

Nine rose diagrams were constructed for convergent flakes for Type 1 edge damage, Type 2 edge damage, and Type 1 and Type 2 edge damage combined. Furthermore, for each type of edge damage, rose diagrams were constructed based on the dorsal face, the ventral face (orientation un-flipped), or dorsal and ventral (ventral orientation flipped around the longitudinal axis to create a composite of edge damage location) combined (Table 2).

In order to analyze specific faces for edge damage, the rose diagrams illustrating one face (dorsal or ventral) portray true orientation data. This means that the degrees representing edge damage were not flipped and the diagrams illustrate damage as if viewing the flake in one's hand. However, because one goal is to create two-dimensional visual images that can represent three-dimensional objects, the degree orientation for ventral flakes is flipped when combined with degrees for dorsal flakes (for example, 5° becomes 355° or 180° becomes 90°). When a tool edge is used for a particular action, both faces of the tool may be affected; the purpose of flipping the ventral degrees is to ascertain which lateral edge was being used most often.

9. Type 1 edge damage

Visually, Type 1 edge damage (retouch) on the ventral faces (un-flipped) of convergent flakes (Fig. 3a) appears to display a non-random distribution. However, sample size (2) and number of angles (230) is too small to obtain an accurate range of

Table 2
Types of edge damage

Type 1 edge damage
Dorsal
Ventral (un-flipped)
Dorsal + ventral (flipped)
Type 2 edge damage
Dorsal
Ventral (un-flipped)
Dorsal + ventral (flipped)
Type 1 + Type 2 edge damage
Dorsal
Ventral (un-flipped)
Dorsal + ventral (flipped)

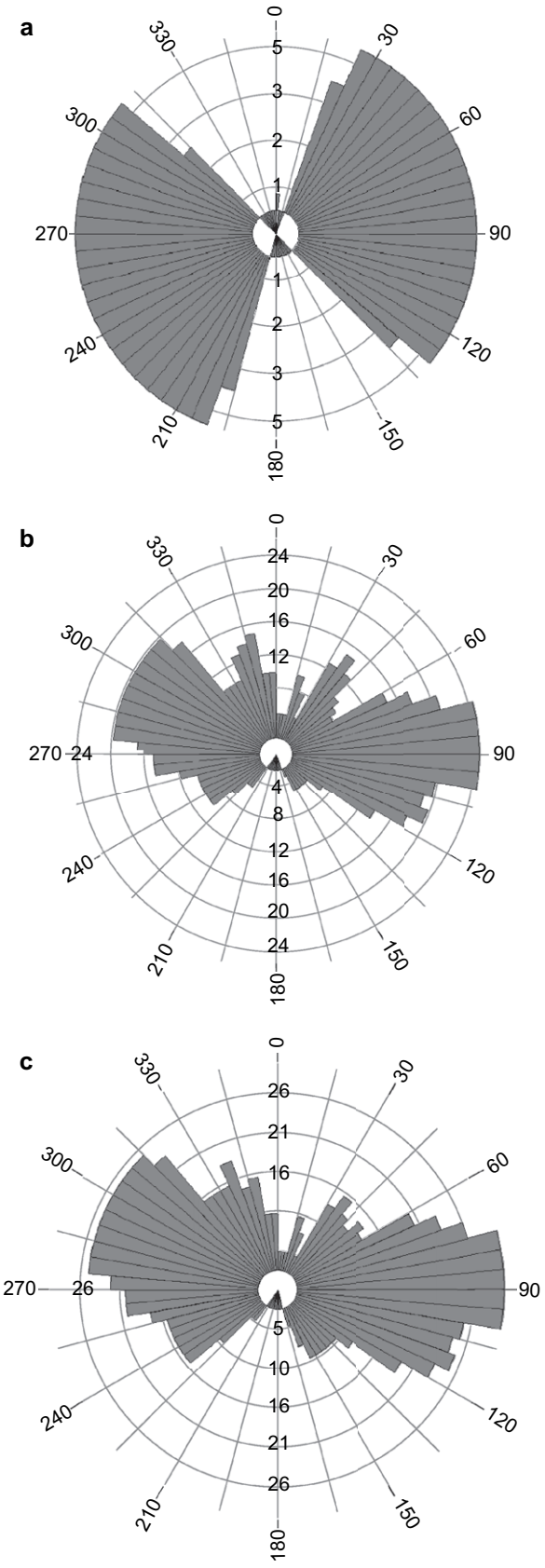

Fig. 3. Rose diagrams of (a) Type 1 edge damage (retouch) on ventral faces, (b) Type 1 edge damage (retouch) on dorsal faces, and (c) Type 1 edge damage (retouch) on dorsal and ventral (flipped) faces.

distributions (Table 3). The Kuiper's V indicates a non-random distribution ($V = 2.94$), these data are above the threshold for rejecting the null hypothesis; Rayleigh's Z falls under a value of 1.0.

Type 1 edge damage distribution on the dorsal faces of convergent flakes (Fig. 3b) includes a sample size of seven faces with a total of 809 angles and displays a non-random distribution on both the left and the right lateral edges (Table 3). The concentration of edge damage lies between 70° and 120° on the right side and between 270° and 325° on the left side. Sixteen angles signifying that damage occurs in this range and 24 angles occur between 75° and 100°. Edge damage is absent along the tip and platform, although the upper right and left lateral edges do show slight projections independent of the mid-lateral edges. Kuiper's V indicates a non-random distribution ($V = 6.802$), as does Rayleigh's Z ($Z = 39.819$, $p < 0.01$).

Combining Type 1 edge damage distributions for the dorsal faces and the ventral (flipped orientation) faces (Fig. 3c), displays a non-random distribution. Damage is concentrated along the lateral edges, bisecting the points longitudinally above and along the centroid. On the right side, the greatest amount of edge damage appears between 60° and 125° with 16 point faces displaying damage in this range and 31 point faces showing damage between 75° and 100°. On the left side, the concentration of damage is between 255° and 320°, with 25 point faces showing damage between 275° and 315°. Although the damage has its highest concentrations on mid-centroid lateral edges, the damage does occur to a lesser extent continuously from 0° to 165° and from 210° to 360°. Kuiper's V indicates a non-random distribution ($V = 6.56$), as does Rayleigh's Z ($Z = 29.248$, $p < 0.01$).

10. Type 2 edge damage

Type 2 edge damage (unknown agent) on the ventral faces (un-flipped orientation) of convergent flakes (Fig. 4a) displays a non-random distribution. The sample size is larger (18 faces) and includes 770 angles (Table 3). Damage is concentrated along two short regions on the right side of the flakes: between 25° and 50° (frequency: 15–19 angles) and between 85° and 120° (frequency: 19–27 angles). Damage occurs less frequently on the left side of the flake, with the majority of the damage between 225° and 270° (frequency: 15–19 angles) and the upper left lateral side (335–345°; frequency: 13–20 angles). The damage is concentrated on the lower right and left lateral edges, just below the longitudinal intersection with the centroid. Kuiper's V supports a non-random distribution ($V = 6.626$), as does Rayleigh's Z ($Z = 27.15$, $p < 0.01$).

Type 2 edge damage on the dorsal faces of convergent flakes (Fig. 4b) displays a non-random distribution pattern. The sample size is large (19 faces) and includes a large (1376) number of angles (Table 3). Damage is concentrated on the left side of the points, particularly in the 200–350° range (frequency: 26–43 angles). The right side of the points are represented on fewer faces, with 7–18 faces displaying damage between 0° and 105° and 24–28 flake faces showing damage between 60° and 80°. This damage on the left side of

Table 3
Kuiper's V and Rayleigh's Z for quartzite convergent flakes (points) from Pinnacle Point 13B

Convergent flakes								
Category	# of faces	# of angles	Kuipers V	Kuipers P	Rejected	Rayleighs' Z	Rayleighs' P	Rejected
T^1 Ventral (un-flipped)	2	230	2.94	<0.01	Yes	0.131	0.877	No
T^1 Dorsal	7	809	6.802	<0.01	Yes	39.819	<0.01	Yes
T^1 D + V (flipped)	9	1039	6.56	<0.01	Yes	29.248	<0.01	Yes
T^2 Ventral (un-flipped)	18	770	6.626	<0.01	Yes	27.15	<0.01	Yes
T^2 Dorsal	19	1376	9.341	<0.01	Yes	176.405	<0.01	Yes
T^2 D + V (flipped)	37	2146	10.232	<0.01	Yes	186.353	<0.01	Yes
$T^1 + T^2$ Ventral (un-flipped)	20	1000	6.763	<0.01	Yes	19.385	<0.01	Yes
$T^1 + T^2$ Dorsal	26	2185	10.4	<0.01	Yes	178.374	<0.01	Yes
$T^1 + T^2$ D + V (flipped)	46	3185	11.723	<0.01	Yes	182.916	<0.01	Yes

the dorsal face of the points, spanning above and below the longitudinal bisection of the centroid, is statistically well-supported with a Kuiper's V ($V = 9.341$) and Rayleigh's Z ($Z = 176.405$) values rejecting the null hypotheses ($p < 0.01$).

Combining Type 2 edge damage distributions for the dorsal faces and the ventral faces (flipped orientation) (Fig. 4c) also results in a non-random distribution pattern. The edge damage is concentrated on the left side of the points. The range of damage on the left side spans from 225° to 360° (frequency: 32–65 angles), with the longest petal of 270–275° (frequency 65 angles). Edge damage on the right side does not occur to the same extent as on the left side, with sporadic petal lengths and greatest frequency (34–43 angles) between 60° and 80°. This left side dominant pattern, spanning above and below the longitudinal bisection of the centroid, is significant as Kuiper's V ($V = 10.232$) and Rayleigh's Z ($Z = 186.353$) values reject the null hypotheses ($p < 0.01$). This pattern is consistent with usewear rather than taphonomic edge damage.

11. Type 1 and Type 2 edge damage combined

When Type 1 and Type 2 edge damage on the ventral face of (un-flipped) convergent flakes are combined (Fig. 5a), the distribution is moderately non-random. The number of faces is large (20) as is the number of angles (1000). On the right side, damage is greatest between 70° and 120° (frequency: 25–32 angles), although a small concentration occurs 25°–50° (frequency 20–23 angles) as well. The left side is patterned similarly on the lower left side between 225° and 300° (frequency: 21–24 angles). Distribution occurs predominantly on the left and right lower laterals, along the longitudinal axis with the centroid and just below. Statistical analysis of this distribution allows rejection of the null hypothesis for Kuiper's V ($V = 6.763$) and for Rayleigh's Z ($Z = 19.385$, $p < 0.01$).

Type 1 and Type 2 edge damage on dorsal convergent flakes combined (Fig. 5b) show a non-random distribution both visually and statistically (Kuiper's $V = 10.4$ and Rayleigh's $Z = 178.374$, $p < 0.01$). Edge damage is concentrated on the left side of the flake, between 260° and 320° (frequency 61 angles). A second concentration occurs on the upper lateral edges between 340° and 350° (frequency: 54 angles). Edge damage is concentrated on the left side as well, with the longest petals ranging from 60° to 80° (frequency: 45–52 angles). With the overwhelming visual evidence of edge damage distribution on the left side of dorsal flakes, we can infer that this area of the convergent flake was most frequently selected for use.

Type 1 and Type 2 edge damage combined for dorsal and ventral (flipped) convergent flakes (Fig. 5c) show a non-random distribution both visually and statistically (Kuiper's $V = 11.723$ and Rayleigh's $Z = 182.916$, $p < 0.01$). Edge damage predominantly lies on the left side of the flake (on both the dorsal side and the ventral side flipped), between 245° and 320° (frequency: outer ring from 64–85 angles), with a slight concentration from 340° to 350° (frequency: over 64 angles). The right side does display edge damage, from 60° to 100° (frequency 46–68 angles), but these long bars are not distributed over a large area and the pattern is not as strong as on the left side of the flake. This predominance of long bars spread over a large area indicates that both Type 1 and Type 2 edge damage are occurring on the left side of the flake (in dorsal view).

12. Discussion

In the cases examined here, the image-based method we have described was very effective at capturing the distribution of edge damage for each artifact, and then compiling those data into an assemblage-level pattern of edge damage distribution. Those data, when summarized by rose diagrams and statistics illustrate that for convergent flakes (points), Type 1 and Type 2 edge damage are non-random. The rose diagrams are also quite effective at illustrating on which edges (left vs. right) there is more edge damage, and where it is absent.

There is an overall absence of edge damage along the platform. This could be due to its thickness and obtuse edge angle in comparison to the rest of the flake. However, it is known that circum-platform damage does result from platform to haft forceful contact during use of a hafted point either as a projectile, stabbing, or cutting implement (Lombard et al., 2004; Lombard, 2005a,b; Rots, 2005; Rots and Van Peer, 2006; Shea, 1997). There is also a lack of damage along the far upper lateral edges, along the tip, and on the edges just above the platform. Coded impact fractures were not included in this analysis, although they are present in the assemblage.

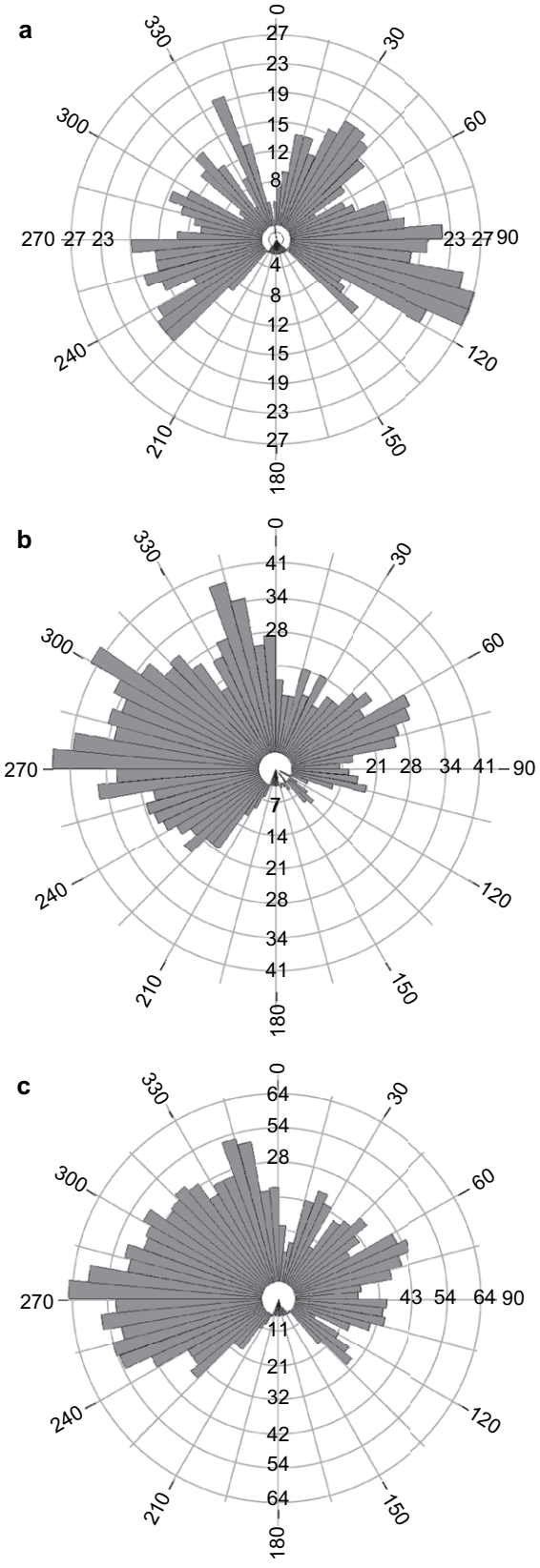

Fig. 4. Rose diagrams of (a) Type 2 edge damage (unknown agent) on ventral faces, (b) Type 2 edge damage (unknown agent) on dorsal faces, and (c) Type 2 edge damage (unknown agent) on dorsal and ventral (flipped) faces.

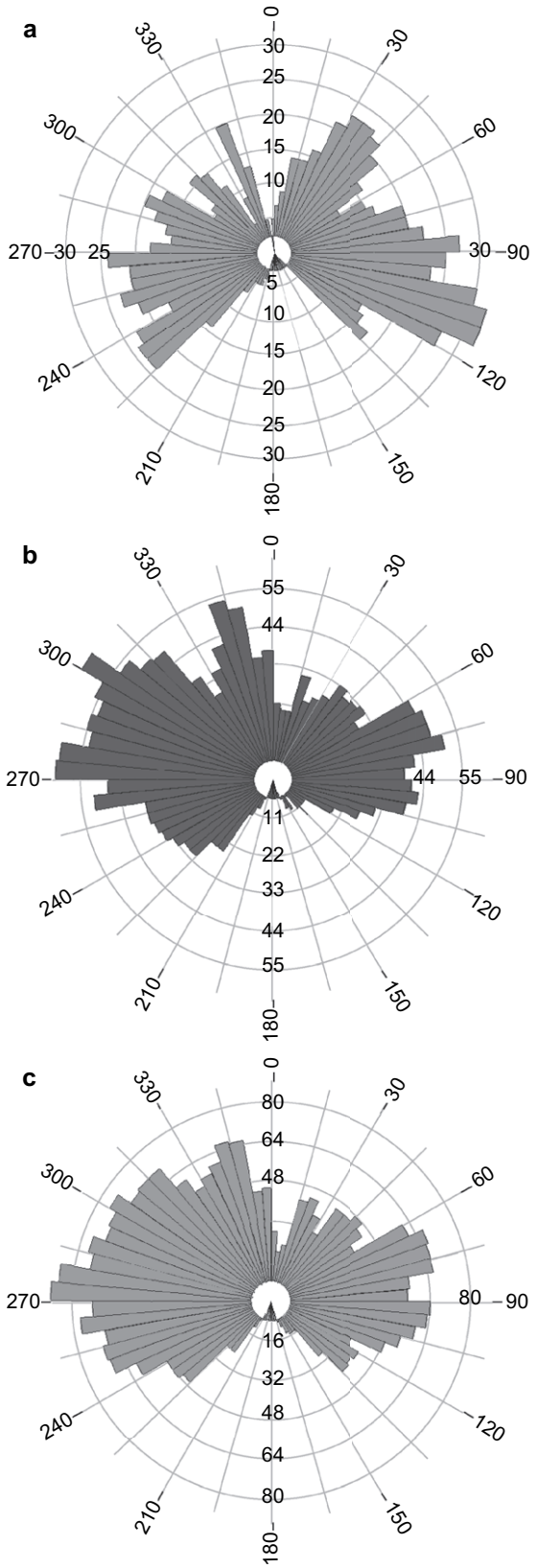

Fig. 5. Rose diagrams of (a) Type 1 (retouch) and Type 2 (unknown agent) edge damage combined on ventral faces, (b) Type 1 (retouch) and Type 2 (unknown agent) edge damage combined on dorsal faces, and (c) Type 1 (retouch) and Type 2 (unknown agent) edge damage combined on dorsal and ventral (flipped) faces.

This was because the impact factures would have obscured the distribution of usewear or taphonomic edge damage. The impact fractures in this assemblage uniformly originate at the distal end and are often burinated (Minichillo, 2005).

The visual and statistical tests of Type 1 edge damage support the original coding as intentional human modification. Type 2 edge damage also is patterned in a non-random way. This type of damage concentrated on the left side of the dorsal faces of the points, spanning above and below the longitudinal bisection of the centroid, is one of the most statistically well-supported patterns. The distribution of Type 2 edge damage patterned on the left side of the assemblage-grouped flakes suggests that the majority of damage was created by either use or retouch, and that handedness coupled to a consistent positional manner of using points may play a role in structuring this pattern. This interesting pattern is revealed by the assemblage-level approach illustrated here.

13. Conclusions

It is difficult to record and analyze patterns of edge damage and retouch on stone tools without oversimplifying the data. As presented in this paper, recording those patterns in a graphical manner on rectified images has many strengths. It provides an archival record that can be re-analyzed in a variety of ways in the future since it presents a near-perfect 2-dimensional record of the artifact. In the future, developing a 3-dimensional approach could be useful. Graphical summaries using polar diagrams and polar statistical analyses of retouch and edge damage, as illustrated here, can provide a basis for examining questions of both function and taphonomy.

Furthermore, the images created can be additive in analysis. For example, with these same specimens we could add to the images positional information on residues (Lombard et al., 2004; Lombard, 2005a) and microwear (Shea, 1997), and analyze the spatial relations of all three in tandem. Metrical analyses can be conducted directly onto the images, new measurements taken without revisiting the assemblage itself, and sharing the assemblage with other scientists electronically becomes possible.

Natural and cultural formation processes, especially repeated occupations of the same locality, can significantly affect artifacts. Teasing these formation processes apart for individual artifacts is a difficult task, which is why it may be more practical to identify overall trends on assemblage-level scales. When applied to specific shape categories, the image-based method we have described here, coupled with assemblage-level pattern recognition techniques, such as rose diagrams, are particularly useful in visually illustrating if edge damage is random or not, and on which face or lateral edges the damage is occurring most frequently.

Acknowledgements

This project was made possible by the Mossel Bay Archaeology Project, Curtis W. Marean and Peter J. Nilssen, directors, and funded by National Science Foundation Grant BCS-0130713 to Marean with REU supplement for Bird, Wenner-Gren Dissertation Fieldwork Grant GR 6894 to Minichillo, and the Hyde Family Trust. We gratefully acknowledge the academic and financial support of the Barrett Honors College at Arizona State University. Michael Barton, Jocelyn Bernatchez, Erin Thompson, Margaret Nelson, and Steve Swanson, Arizona State University, and Angela Close, University of Washington, provided useful assistance and comments. Three anonymous reviewers provided useful comments that improved the quality of the paper.

References

Barham, L., 2000. The Middle Stone Age of Zambia, South Central Africa. Western Academic & Specialist Press, Bristol.

Barton, M., Clark, G., 1993. Cultural and natural formation processes in late Quaternary cave and rockshelter sites of Western Europe and the Near East. In: Goldberg, P., Nash, D.T., Petraglia, M.D. (Eds.), Formation Processes in Archaeological Context. Prehistory Press, Madison, Wisconsin, pp. 33–52.

Bordes, F., 1961. Mousterian cultures in France. Sci. 134, 803–810.

Deacon, H.J., Deacon, J., 1999. Human Beginnings in South Africa: Uncovering the Secrets of the Stone Age. Alta Mira Press, Walnut Creek.

Debénath, A., Dibble, H.L., 1994. Handbook of Paleolithic Typology: Lower and Middle Paleolithic of Europe. University Museum, University of Pennsylvania, Philadelphia.

Fisher, N.I., 1993. Statistical Analysis of Circular Data. Cambridge University Press, London.

Flenniken, J., Haggerty, J., 1979. Trampling as an agent in the formation of edge damage: an experiment in lithic technology. NW Anthropol. Res. Notes 13, 208–214.

Gifford-Gonzalez, D.P., Damrosch, D.B., Damrosch, D.R., Pryor, J., Thunen, R.L., 1985. The third dimension in site structure: an experiment in trampling and vertical dispersal. Am. Antiq. 50, 803–818.

Henshilwood, C.S., d'Errico, F., Marean, C.W., Milo, R., Yates, R., 2001. An early bone tool industry from the Middle Stone Age at Blombos Cave, South Africa: implications for the origins of modern human behavior, symbolism, and language. J. Hum. Evol. 41, 631–678.

Henshilwood, C.S., d'Errico, F., Yates, R., Jacobs, Z., Tribolo, C., Duller, G.A.T., Mercier, N., Sealy, J.C., Valladas, H., Watts, I., Wintle, A., 2002. Emergence of modern human behavior: Middle Stone Age engravings from South Africa. Sci. 295, 1278–1280.

Henshilwood, C., d'Errico, F., Vanhaeren, M., van Niekerk, K., Jacobs, Z., 2004. Middle Stone Age shell beads from South Africa. Sci. 304, 404.

Henshilwood, C.S., Marean, C.W., 2003. The origin of modern human behavior: critique of their models and test implications. Curr. Anthropol. 44, 627–652.

Keeley, L.H., 1980. Experimental Determination of Stone Tool Uses: A Microwear Analysis. University of Chicago Press, Chicago.

Klein, R.G., 1992. The archaeology of modern human origins. Evol. Anthropol. 1, 5–12.

Klein, R.G., 1999. The Human Career: Human Biological and Cultural Origins, second ed. University of Chicago Press, Chicago.

Lombard, M., Parsons, I., van der Ryst, M.M., 2004. Middle Stone Age lithic point experimentation for macro-fracture and residue analyses: the process and preliminary results with reference to Sibudu Cave points. S. Afr. J. Sci. 100, 159–166.

Lombard, M., 2005a. Evidence of hunting and hafting during the Middle Stone Age at Sibudu Cave, KwaZuluNatal, South Africa: a multianalytical approach. J. Hum. Evol. 48, 279–300.

Lombard, M., 2005b. A method for identifying Stone Age hunting tools. S. Afr. Archaeol. Bull. 60, 115–120.

Marean, C.W., Nilssen, P., Brown, K., Jerardino, A., Stynder, D., 2004. Paleoanthropological investigations of Middle Stone Age sites at Pinnacle Point,

Mossel Bay (South Africa): archaeology and hominid remains from the 2000 field season. Paleoanthropology, 14–83.

McBrearty, S., Brooks, A., 2000. The revolution that wasn't: a new interpretation of the origin of modern human behavior. J. Hum. Evol. 39, 453–563.

McBrearty, S., Bishop, L., Plummer, T., Dewar, R., Conard, N., 1998. Tools underfoot: human trampling as an agent of lithic artifact edge modification. Am. Antiq. 63, 108–129.

McDougall, I., Brown, F.H., Fleagle, J.G., 2005. Stratigraphic placement and age of modern humans from Kibish, Ethiopia. Nature 433, 733–736.

Minichillo, T.J., 2005. Middle Stone Age Lithic Study, South Africa: An Examination of Modern Human Origins. Unpublished doctoral dissertation, University of Washington, Seattle.

Mitchell, P., 2002. The Archaeology of Southern Africa. Cambridge University Press, Cambridge.

Newcomer, M.H., 1976. Spontaneous retouch. In: Engelsen, G.H.G. (Ed.), Second International Symposium on Flint, Staringia 3, Maastricht, pp. 62–64.

Nielsen, A.E., 1991. Trampling the archaeological record: an experimental study. Am. Antiq. 56, 483–503.

Pryor, J.H., 1988. The effects of human trample damage on lithics: a model of crucial variables. Lith. Tech. 17, 45–50.

Rots, V., 2005. Wear traces and the interpretation of stone tools. J. Field Archaeol. 30, 61–73.

Rots, V., Van Peer, P., 2006. Early evidence of complexity in lithic economy: core-axe production, hafting and use at the Late Middle Pleistocene site 8-B-11, Sai Island (Sudan). J. Archaeol. Sci. 33, 360–371.

Shea, J.J., Klenck, J.D., 1993. An experimental investigation of the effects of trampling on the results of lithic microwear analysis. J. Archaeol. Sci. 20, 175–194.

Shea, J.J., 1997. Middle Paleolithic spear point technology. In: Knecht, H. (Ed.), Projectile Technology. Plenum Press, New York, pp. 79–106.

Shea, J.J., 2006. The origins of lithic projectile point technology: evidence from Africa, the Levant, and Europe. J. Archaeol. Sci. 33, 823–846.

Singer, R., Wymer, J., 1982. The Middle Stone Age at Klasies River Mouth in South Africa. University of Chicago Press, Chicago.

Thackeray, A.I., 1992. The Middle Stone Age south of the Limpopo River. J. World Prehist. 6, 385–440.

Tringham, R., Cooper, G., Odell, G., Voytek, B., Whitman, A., 1974. Experimentation in the formation of edge damage: a new approach to lithic analysis. J. Field Archaeol. 1, 171–196.

Tryon, C.A., McBrearty, S., 2006. Tephrostratigraphy of the Bedded Tuff Member (Kapthurin Formation, Kenya) and the nature of archaeological change in the later middle Pleistocene. Quat. Res. 65, 492–507.

Vaughan, P.C., 1985. Use-Wear Analysis on Flaked Stone Tools. University of Arizona Press, Tucson.

Villa, P., Delagnes, A., Wadley, L., 2005. A late Middle Stone Age artifact assemblage from Sibudu (KwaZulu-Natal): comparisons with the European Middle Paleolithic. J. Archaeol. Sci. 32, 399–422.

Volman, T.P., 1981. The Middle Stone Age in the southern Cape. Unpublished doctoral dissertation, University of Chicago, Chicago.

Wadley, L., Vogel, J.C., 1991. New dates from Rose Cottage Cave. S. Afr. J. Sci. 87, 605–608.

White, T.D., Asfaw, B., DeGusta, D., Gilbert, H., Richards, G.D., Suwa, G., Howell, F.G., 2003. Pleistocene Homo sapiens from Middle Awash, Ethiopia. Nature 423, 742–747.

Wurz, S., 2002. Variability in the Middle Stone Age lithic sequence, 115,000 years ago at Klasies River, South Africa. J. Archaeol. Sci. 29, 1001–1015.

Wurz, S., le Roux, N., Gardner, S., Deacon, H.J., 2003. Discriminating between the end products of the earlier Middle Stone Age sub-stages at Klasies River using biplot methodology. J. Archaeol. Sci. 30, 1107–1126.

Wurz, S., Van Peer, P., le Roux, N., Gardner, S., Deacon, H.J., 2005. Continental patterns in stone tools: a technological and biplot-based comparison of early Late Pleistocene assemblages from northern and southern Africa. Afr. Archaeol. Rev. 22, 1–24.

Yellen, J.E., 1996. Behavioral and taphonomic patterning at Katanda 9: a Middle Stone Age site, Kivu Province, Zaire. J. Archaeol. Sci. 23, 915–932.